Volume 6, Issue 1, 062503 (1-9)

Fuzzy Optimization and Modeling Journal (FOMJ)

https://doi.org/10.57647/j.fomj.2025.8667

A blended model based on fuzzy logic for the calculation of Reynolds Stresses in turbulent flows

Mohsen Fatehi*

Faculty of Engineering, Free University of Bolzano, Bolzano, Italy.

***Corresponding author:** mofatehi@unibz.it

Original Research

Received:
28 February 2025
Revised:
18 March 2025
Accepted:
25 March 2025
Published online:
23 April 2025

Abstract:

A novel blended model for turbulent stresses is hereby introduced, combining two well-established turbulence models: the $k-\varepsilon$ model and the explicit algebraic stress model of Wallin and Johansson (WJ). The blending of these models can be implemented in two ways: a binary approach, where the $k-\varepsilon$ model is used for shear stresses and the explicit algebraic stress model for normal stresses; or a fuzzy approach, which integrates both models in a more flexible manner. The model is implemented by formulating the momentum equations based on the $k-\varepsilon$ model and incorporating additional momentum source terms from the blended formulation. This approach leverages the strengths of both $k-\varepsilon$ and algebraic stress models, enhancing accuracy while maintaining computational efficiency. CFD simulations of a benchmark case, a backward-facing step, demonstrate that both the binary and fuzzy implementations effectively predict turbulent normal and shear stresses. The findings indicate that the blended model exhibits superior performance in terms of accuracy when compared with both the $k-\varepsilon$ model and the explicit algebraic model. Furthermore, the fuzzy approach yielded the most precise results, surpassing those of the $k-\varepsilon$ model, WJ model, and binary model. In terms of computational cost, the fuzzy and binary blended models require 1.58 and 1.56 times the CPU time of the $k-\varepsilon$ model, respectively, while the WJ model is the most computationally expensive, requiring 1.76 times the CPU time of the $k-\varepsilon$ model.

Keywords: Turbulence models; Algebraic stress; Two-equation models; Fuzzy logic; Backward facing step

1. Introduction

Turbulence modelling is a significant component of flow simulations in fluid flows. The majority of prevalent turbulence models are founded on suitable approximations of the precise Navier-Stokes equations, specifically the Reynolds-averaged Navier-Stokes equations (RANS). The fundamental starting point of this modelling is the Reynolds decomposition of the flow variables into mean and fluctuating parts. The insertion of the Reynolds-decomposed variables into the governing equations, followed by an averaging of the equations themselves, gives rise to the Reynolds-stress tensor and turbulent fluxes. These unknown terms must then be modelled in terms of the flow field primary variables. The problem of closing the system of Navier–Stokes equations essentially addresses this task.

Osborne Reynolds [1] introduced the Reynolds decomposition and averaging of the Navier–Stokes equations. The concept of eddy viscosity for the modelling of the Reynolds-stress tensor was the first remedy for the closure problem [2]. The first successful calculation of a practical turbulent flow was achieved in the 1920s by Prandtl [3], who introduced the concept of mixing length for the determination of the eddy viscosity. The use of the turbulent kinetic energy transport equation opened the way to the one-equation models, where the turbulence length scale is defined empirically, and the turbulent kinetic energy is obtained from a specific transport equation. More widely used are the two-equation models, in particular the $k-\varepsilon$ model [4], where transport equations for the turbulent kinetic energy and the energy-dissipation rate are used. The eddy viscosity assumption, however, suffers from several drawbacks intrinsic to all the one- and two-equation models, such as the inability to properly account for streamline curvature, body forces, and history effects on the individual components of the Reynolds-stress tensor.

In search for a better presentation of the turbulence model, Rotta [5] gave a fundamental contribution to a full Reynolds stress turbulence closure and introduced the second order, or “second moment”, models. The models based on the Reynolds-stress transport equation are usually able to account for history and nonlocal effects on the evolution of

the components of the Reynolds-stress tensor. Nonetheless, because they require the solution of six additional transport equations for the individual components of the Reynolds-stress tensor, it has not been computationally feasible until the 1970s to solve complex engineering flows based on full second-order closures. Among the first works embodying second-order closure models is that of Launder et al. [6] who developed a second-order closure model (the Launder, Reece, and Rodi (LRR) model) that significantly improves the work of Rotta [5]. Lumley [7] implemented the constraint of realizability and gave significant contributions to the modelling of the pressure-strain correlation. Launder [8] continued the work of applying second-order closures to problems of engineering interest. Speziale [9, 10] exploited invariance arguments and consistency conditions for the solutions of the system of the Navier–Stokes equations to develop new models for the rapid pressure-strain correlation. Haworth and Pope [11] developed a second-order closure model by following a fundamental approach.

Despite the advancement of computers and computational algorithms, second-order closure models (RSM) still impose a heavy computational burden on the numerical simulation of turbulent flows. Attempts to reduce the differential RSM equations to a set of algebraic equations, pioneered by Launder and Rodi [6] have led to the Algebraic Stress Models (ASM). Rodi [12] described a new algebraic expression relating the Reynolds stress to the mean velocity. Speziale et al. [13] proposed a linear model for pressure-strain correlation in the context of an ASM, which led to the explicit algebraic SSG model. Wallin and Johansson [14] presented another explicit ASM for two- and three-dimensional turbulent flows. The ASM variants are simpler and more amenable to numerical algorithms than the RSM, but still inferior to the eddy-viscosity models in terms of the computational economy.

The attractive features of computational economy and convergence behaviour of two-equation models, and their successful predictions in shear-dominated flows, and the simplicity and ability to account for the anisotropy of turbulence of the ASM, motivates one to take advantage of both models in a hybrid approach. The first attempt at such a hybrid model is due to Davidson [15] whose model takes from an ASM that part of the non-isotropic Reynolds stress which is due to buoyancy, and the remaining part from the $k-\varepsilon$ model. The model is tested in a buoyancy-driven cavity flow. The contributions from the ASM corrections to the Reynolds stress and the turbulent heat flux are up to five and ten times, respectively, larger than those from the $k-\varepsilon$ model. Menter [16] combined different elements of two-equation eddy viscosity turbulence models of $k-\omega$ and $k-\varepsilon$ models. This model utilizes the original $k-\omega$ model of Wilcox [17] in the inner region of the boundary layer and switches to the $k-\varepsilon$ model in the outer region and free shear flow. Also, in recent years, the blending concept has proven useful in the development of turbulence models. There are also studies which have explored the blending of the $k-\varepsilon$ model with Algebraic Stress Models (ASM) to improve turbulence predictions in complex flows. Khaleghi and Fallah [18] investigated iterative and non-iterative solutions using ASM and $k-\varepsilon$ models, sho wing that ASM can enhance the accuracy of standard $k-\varepsilon$ models in engine flow simulations. Similarly, Basara and Jakirlic [19] proposed a hybrid turbulence model combining the Reynolds stress model with the $k-\varepsilon$ model. Their approach improves computational efficiency while maintaining the physical accuracy of the Reynolds-stress model, offering a more reliable solution for complex turbulent flows. These studies highlight the advantages of hybrid models in enhancing turbulence modeling accuracy and computational efficiency. C. Eric Lynch [20] evaluated the ability of a hybrid Reynolds-Averaged Navier-Stokes (RANS) and Large Eddy Simulation (LES) turbulence to accurately predict the physics of an unsteady separated flow field. The hybrid method consists of a blending of the $k-\omega$ SST RANS model with a one-equation LES model. Islam [21] has developed a new hybrid turbulence model. The model combines Implicit Large-Eddy Simulation and Reynolds-Averaged Navier-Stokes. This method of a continuous, non-zonal approach with a hybrid blending function operating at the edge of boundary layers and separated flow regions.

The present work claims to be the first approach in which the two-equation $k-\varepsilon$ and the WJ [14] models are combined in a binary way and a fuzzy way to use the favourable features of both turbulence models. The following sections describe the features of the combined models and their validations against experimental sets of data.

2. The governing equations

The Reynolds-averaged Navier-Stokes equations for incompressible flows are the main governing equations, which may be written as follows [22]:

$$\frac{\partial \bar{u}_i}{\partial x_i} = 0 \tag{1}$$

$$\rho\left(\frac{\partial \bar{u}_i}{\partial t} + \bar{u}_j\frac{\partial \bar{u}_i}{\partial x_j}\right) = \bar{B}_i - \frac{\partial \bar{p}}{\partial x_i} + \frac{\partial}{\partial x_j}\left(\mu\frac{\partial \bar{u}_i}{\partial x_j}0 - \rho\overline{\acute{u}_i\acute{u}_j}\right) \tag{2}$$

where u_i is the fluid mean velocity, p is the mean pressure, ν is the fluid kinematic viscosity, and $\bar{B}_i$ is the mean body force. The apparent extra-stress term on the right-hand-side of the momentum equation, is referred to as the Reynolds stress, and should be modelled via an appropriate turbulence model. As we only concern with the two-equation models and the algebraic stress models, these models are explained in the following sub-sections. Interested readers may consult [22] for an exhaustive review on other turbulence models.

2.1 The standard $k-\varepsilon$ model

This model is based on the eddy viscosity assumption of [2], in which the effect of turbulence on the flow-field may be taken into account by relating the mean velocity gradients to the Reynolds stresses through a turbulent eddy viscosity coefficient [23]. Usually, a linear relation of the following form is considered:

$$-\overline{\rho\acute{u}_i\acute{u}_j} = -\bar{\rho}\nu_t S_{ij} - \frac{2}{3}\bar{\rho}k\delta_{ij} \tag{3}$$

$$S_{ij} = \frac{1}{2}\left(\frac{\partial \bar{u}_i}{\partial x_j} + \frac{\partial \bar{u}_j}{\partial x_i}\right) \tag{4}$$

where $k = 1/2\overline{\acute{u}_i\acute{u}_j}$ is the specific kinetic energy of turbulence, ν_t is the turbulence eddy kinematic viscosity, and δ_{ij} is the Kronecker delta.
Substitution of Eq. (3) in the momentum equation results:

$$\bar{\rho}\frac{\partial \bar{u}_i}{\partial t} + \overline{\rho u_i}\frac{\partial \bar{u}_i}{\partial x_j} = -\frac{\partial}{\partial x_i}(P_{eff}) + \frac{\partial}{\partial x_i}(\bar{\rho}\nu_{eff}S_{ij}) \tag{5}$$

where:

$$\nu_{eff} = \nu + \nu_t \tag{6}$$

$$P_{eff} = P + \frac{2}{3}\bar{\rho}k \tag{7}$$

In the above equations, ν is the kinematic viscosity of the fluid, ν_{eff} is the effective kinematic viscosity, and P_{eff} is the effective pressure.
The $k-\varepsilon$ model calculates turbulence kinematic viscosity from [23]:

$$\nu_t = C_\mu \frac{k^2}{\varepsilon} \tag{8}$$

where C_μ is the correlation constant, k and ε are, respectively, the kinetic energy of turbulence and its dissipation. The transport equations for k and ε may be written as [23]:

$$\bar{\rho}\frac{Dk}{Dt} = \frac{\partial}{\partial x_i}\left[\bar{\rho}\left(\nu + \frac{\nu_t}{\sigma_k}\right)\frac{\partial k}{\partial x_i}\right] + P_g - \bar{\rho}\varepsilon \tag{9}$$

$$\bar{\rho}\frac{D\varepsilon}{Dt} = \frac{\partial}{\partial x_i}\left[\bar{\rho}\left(\nu + \frac{\nu_t}{\sigma_\varepsilon}\right)\frac{\partial \varepsilon}{\partial x_i}\right] + C_{\varepsilon 1}\frac{\varepsilon}{k}P_g - C_{\varepsilon 2}\bar{\rho}\frac{\varepsilon^2}{k} \tag{10}$$

where $P_g = -\overline{\rho\acute{u}_i\acute{u}_j}(\partial \bar{u}_i/\partial x_j)$ is the production term, $C_{\varepsilon 1}$ and $C_{\varepsilon 2}$ are the model constants, and σ_k and σ_ε are the turbulence Prandtl numbers of k and ε, respectively. The following set of data is used for the constants of $k-\varepsilon$ model [23]:

$$C_\mu = 0.09,\ \ \sigma_k = 1,\ \ \sigma_\varepsilon = 1.3,\ \ C_{\varepsilon 1} = 1.44,\ \ C_{\varepsilon 2} = 1.92 \tag{11}$$

2.2 The algebraic stress model

The ASM is a simplified version of Reynolds Stress Model (RSM), in which the differential transport equations of the Reynolds stress tensor components are reduced to a set of algebraic equations. The ASM of turbulent stress is written as [6]:

$$\bar{\rho}\frac{\overline{\acute{u}_i\acute{u}_j}}{k}(P_g - \varepsilon) = \bar{\rho}(P_{ij} - \varepsilon_{ij} + \acute{\phi}_{ij}) \tag{12}$$

where P_{ij} and ε_{ij} are, respectively, the production and dissipation terms associated to $\overline{\acute{u}_i\acute{u}_j}$, and $\acute{\phi}_{ij}$ is the pressure-strain correlation. The above relation is the main relation for algebraic stress models. The only difference between different algebraic models is the pressure-strain correlation and related coefficients. The production term may be written in terms of the mean values as:

$$P_{ij} = -\left[(\overline{\acute{u}_i\acute{u}_k})\frac{\partial \bar{u}_k}{\partial x_j} + (\overline{\acute{u}_j\acute{u}_k})\frac{\partial \bar{u}_k}{\partial x_i}\right] \tag{13}$$

Based on sub-models for the dissipation term and the pressure-strain correlation, different versions of ASM are obtained [12, 14, 24]. Pressure-strain correlation is defined as:

$$\overline{\rho\acute{u}_i\acute{u}_j} = \frac{2}{3}\bar{\rho}\delta_{ij} + \frac{k\bar{\rho}(1-C_2)}{C_1 + \frac{P}{\varepsilon} - 1}\left(\frac{P_{ij}}{\varepsilon} - \frac{2}{3}\frac{P_g}{\varepsilon}\delta_{ij}\right) \tag{14}$$

The above equation is the final form of the LRR algebraic equation for Reynolds stresses, which is used in conjunction with equations of k and ε.
The SSG model defines an anisotropic tensor b_{ij} as [13]:

$$b_{ij} = \frac{\overline{\acute{u}_i\acute{u}_j}}{2k} - \frac{1}{3}\delta_{ij} \tag{15}$$

Upon substitution of b_{ij} in Eq. (12), the following relation is derived:

$$\begin{aligned}(P_g - \varepsilon)b_{ij} = &-\frac{2}{3}kS_{ij} - k(b_{ik}S_{jk} + b_{jk}S_{ik} - \frac{2}{3}b_{mn}S_{mn}\delta_{ij})\\ &- k(b_{ik}W_{jk} + b_{jk}W_{ik}) + \frac{1}{2}\acute{\phi}_{ij}\end{aligned} \tag{16}$$

where $S_{ij} = \frac{1}{2}(\frac{\partial \bar{u}_i}{\partial x_j} + \frac{\partial \bar{u}_j}{\partial x_i})$ is the mean strain tensor and $W_{ij} = \frac{1}{2}(\frac{\partial \bar{u}_i}{\partial x_j} - \frac{\partial \bar{u}_j}{\partial x_i})$ is the mean rotation tensor.
The pressure-strain correlation is expressed by Speziale et al. [13, 24]:

$$\begin{aligned}\acute{\phi}_{ij} = &-C_1\varepsilon b_{ij} + C_2kS_{ij} + C_3k(b_{ik}S_{jk} + b_{jk}S_{ik} - \frac{2}{3}b_{mn}S_{mn}\delta_{ij})\\ &+ C_4k(b_{ik}W_{jk} + b_{jk}W_{ik})\end{aligned} \tag{17}$$

where there are following coefficients in Speziale, Sarkar and Gatski model [13, 24]:

$$\begin{aligned}C_1 = 3.4 + 1.8\frac{P_g}{\varepsilon},\ \ C_2 = 0.8 - 1.3(b_{ij}b_{ij})^{0.5},\\ C_3 = 1.25,\ \ C_4 0.4\end{aligned} \tag{18}$$

Gatski et al. [24] defined the following non-dimensional quantities:

$$S^*_{ij} = \frac{1}{2}(\frac{1}{2}C_1 + \frac{P_g}{\varepsilon} - 1)^{-1}\frac{k}{\varepsilon}(2 - C_3)S_{ij} \tag{19}$$

$$W^*_{ij} = \frac{1}{2}(\frac{1}{2}C_1 + \frac{P_g}{\varepsilon} - 1)^{-1}\frac{k}{\varepsilon}(2 - C_4)W_{ij} \tag{20}$$

$$b^*_{ij} = \frac{(C_3 - 2)}{(C_2 - \frac{4}{3})}b_{ij} \tag{21}$$

$$\eta^2 = (S^*_{ij}S^*_{ij}) \tag{22}$$

$$\xi^2 = (W^*_{ij}W^*_{ij}) \tag{23}$$

By substituting the above relations into Eq. (17), the SSG model of ASM is obtained, which in two-dimensional form may be written as:

$$\begin{aligned}\overline{\rho\acute{u}_i\acute{u}_j} = &\frac{2}{3}k\bar{\rho}\delta_{ij} - \frac{6(1+\eta^2)\alpha_1 k}{3 + \eta^2 + 6\eta^2\xi^2 + 6\xi^2}\\ &\left[S^*_{ij} + (S^*_{ik}W^*_{kj} - W^*_{ik}S^*_{kj}) - 2(S^*_{ik}S^*_{kj} - \frac{1}{3}S^*_{kl}S^*_{kl}\delta_{ij})\right]\end{aligned} \tag{24}$$

where:

$$\alpha_1 = \frac{(C_2 - \frac{4}{3})}{C_3 - 2} \tag{25}$$

$$C_1 = 6.8,\ C_2 = 0.36,\ C_3 = 1.25,\ C_4 = 0.4 \tag{26}$$

WJ model defined the non-isotropic tensor a_{ij} as follows [14]:

$$a_{ij} = \frac{\overline{\acute{u}_i \acute{u}_j}}{k} - \frac{2}{3}\delta_{ij} \tag{27}$$

Therefore, the pressure-strain correlation is expressed via WJ model:

$$\begin{aligned}\acute{\varphi}_{ij} = &-C_1 \varepsilon a_{ij} + \frac{4}{5} k S_{ij} + \frac{9C_2 + 6}{11} k (a_{ik} S_{kj} + S_{ik} a_{kj} \\ &- \frac{2}{3} a_{km} S_{mk} \delta_{ij}) + \frac{7C_2 - 10}{11} k (a_{ik} W_{kj} - W_{ik} a_{kj})\end{aligned} \tag{28}$$

where:

$$S^*_{ij} = \tau S_{ij} = \frac{\tau}{2}\left(\frac{\partial \overline{u}_i}{\partial x_j} + \frac{\partial \overline{u}_j}{\partial x_i}\right) \tag{29}$$

$$W^*_{ij} = \tau W_{ij} = \frac{\tau}{2}\left(\frac{\partial \overline{u}_i}{\partial x_j} - \frac{\partial \overline{u}_j}{\partial x_i}\right) \tag{30}$$

The equation (28) can be written in the following matrix form:

$$\begin{aligned}(C_1 - 1 + \frac{P_g}{\varepsilon})\mathbf{a} = &-\frac{8}{15}\mathbf{S}^* + \frac{7C_2 + 1}{11}(\mathbf{a}\mathbf{W}^* - \mathbf{W}^*\mathbf{a}) \\ &- \frac{5 - 9C_2}{11}(\mathbf{a}\mathbf{S}^* + \mathbf{S}^*\mathbf{a} - \frac{2}{3}\{\mathbf{a}\mathbf{S}^*\}\mathbf{I})\end{aligned} \tag{31}$$

The value of C_2 in the rapid pressure-strain model was originally suggested to be 0.4 by Launder et al. [6], but more recent studies have suggested a higher value close to $5/9$ [14]. This means that the last term in Eq. (31) is of quite small influence. Setting $C_2 = 5/9$ one obtains the simplified but still implicit equation.

$$(C_1 - 1 + \frac{P_g}{\varepsilon})\mathbf{a} = -\frac{8}{15}\mathbf{S}^* + \frac{4}{9}(\mathbf{a}\mathbf{W}^* - \mathbf{W}^*\mathbf{a}) \tag{32}$$

The detailed derivation and model constants are found in [14].

3. Hybrid modelling of $k-\varepsilon$ and ASM

Both the $k-\varepsilon$ model and the ASM model of WJ have been implemented in an in-house computer code. The present approach takes advantage of favorable features of both models, while avoiding their flaws. Two strategies may be pursued for implementing a hybrid model. The first one, which is simpler, is to use a binary switch between the $k-\varepsilon$ model and the WJ model. The second approach is to use fuzzy modelling to combine both the $k-\varepsilon$ and the WJ models.

3.1 The binary model

In this model, the turbulent shear stresses in the whole domain are calculated via the $k-\varepsilon$ model, whereas the normal stresses are evaluated by the WJ model. Such an approach is motivated by the results of numerical simulation of benchmark cases, in which the $k-\varepsilon$ predictions of shear stresses outperforms those of the ASM, but the normal stresses are better predicted by the ASM [13, 23].

In order to take advantage of the better convergence behaviour of the $k-\varepsilon$ model, the momentum equations are written based on the $k-\varepsilon$ model, Eq. (5), while term $-\xi \frac{\partial}{\partial x_j}(\rho \overline{\acute{u}_i \acute{u}_j}_{\text{mod.}})$ is added to the right-hand side, where $\overline{\acute{u}_i \acute{u}_j}_{\text{mod}}$ is defined as:

$$\overline{\acute{u}_i \acute{u}_j}_{\text{mod.}} = \overline{\acute{u}_i \acute{u}_j}_{\text{ASM}} - \overline{\acute{u}_i \acute{u}_k}_{k-\varepsilon} \tag{33}$$

and ξ is a switch parameter, which is 1 when $i = j$ (for normal stresses) and 0 when $i \neq j$ (shear stresses). By substituting expression for the $k-\varepsilon$ and the ASM model in Eq. (33), the following relation for $\overline{\acute{u}_i \acute{u}_j}_{\text{mod.}}$ is obtained:

$$\overline{\acute{u}_i \acute{u}_j}_{\text{mod.}} = \frac{k}{2}[(b_{ij})_{\text{ASM}} - (b_{ij})_{k-\varepsilon}] \tag{34}$$

where b_{ij} is already introduced in Eq. (15) or Eq. (27).

3.2 The fuzzy model

Fuzzy logic is a form of many-valued logic; it deals with reasoning that is fixed or approximate rather than fixed and exact. In contrast with "crisp logic", where binary sets have two-valued logic: true or false, fuzzy logic variables may have a truth value that ranges in degree between 0 and 1. Fuzzy logic has been extended to handle the concept of partial truth, where the truth value may range between completely true and completely false. Furthermore, when linguistic variables are used, these degrees may be managed by specific functions [25].

Fuzzy logic was selected as the adaptive blending technique due to its ability to manage uncertainties, incorporate expert knowledge, and provide smooth transitions between different turbulence models [26]. Unlike other adaptive blending approaches, which often rely on empirical tuning or data-driven optimization, fuzzy logic offers a rule-based framework that ensures flexibility and interpretability. This method prevents abrupt switching between models, reducing numerical instabilities and maintaining physical consistency in turbulent flow predictions. Furthermore, its computational efficiency makes it an attractive alternative to machine learning-based approaches, which typically require large datasets and significant training efforts [27].

Moreover, fuzzy logic provides an adaptive and flexible approach to model blending, where the transition between different models is governed by degrees of membership rather than fixed thresholds. This approach is based on fuzzy set theory, where each input can belong to multiple sets with varying degrees of membership, facilitating smoother transitions [2]. The blending parameter is typically chosen based on physical quantities such as pressure and velocity, which influence the system's behavior. The membership function, often selected as Gaussian or triangular, ensures a gradual and stable transition between models. Compared to conventional blending methods like linear interpolation, fuzzy logic better handles nonlinear systems, offering improved stability and accuracy, though at the cost of increased computational complexity [28].

At this stage, we need a criterion to specify the degree of anisotropy of turbulence to enable us choosing the right turbulence model, or perhaps an appropriate blend of $k-\varepsilon$

and ASM. A good choice is the degree of anisotropy in the anisotropic tensor b_{ij} Eq. (14) or a_{ij} Eq. (27). The difference between the Eigenvalues of this tensor is a measure of the difference between the turbulence normal stresses. Lumley noted that these Eigenvalues are in the range [7].

$$-\frac{1}{3} \leq b^{\alpha} \leq \frac{2}{3} \quad \alpha = 1,\ 2,\ 3 \tag{35}$$

From Eq. (35), it is obvious that the difference between the maximum and minimum Eigenvalues is in the range of 0 and 1. A value close to 1 indicates higher anisotropy, whereas a value close to 0 shows more isotropic turbulence field. The implementation of this model follows the same approach as the binary model. That is, adding a source term $-\xi \frac{\partial}{\partial x_j}(\rho \overline{u_i} \overline{u_j}_{\text{mod.}})$ to the right-hand side of the momentum equation based on the $k-\varepsilon$ model, where parameter ξ controls the weight of modification.

We choose to use the values in Table 1 for ξ based on the difference between the Eigenvalues $\beta \equiv |b^{\alpha}_{\max} - b^{\alpha}_{\min}|$. An in-house computational code is used to perform the numerical simulations. The code is based on the control volume discretization of the governing equations on a collocated grid. The SIMPLE algorithm [29] is used to solve the discretized flow field equations in a sequential order. Pressure-velocity coupling is ensured by the Rhie-Chow interpolation [12] in calculating mass flux across the cell faces. All the terms in the governing partial differential equations are discretized by second-order schemes.

4. Numerical simulation of a Backward-facing step

The backward-facing step is among the standard benchmarks which are used to evaluate turbulence models. Isotropic and anisotropic flow patterns are found in different regions of this type of flow configuration. The present geometry has already been studied experimentally by Kim et al. [30].

Figure 1 shows a schematic of the studied case. The inlet height, $H1$, is two times bigger than the step height ΔH. The flow Reynolds number, based on $H1$, is 132000. In order to reduce possible downstream effects on the simulation, the length of channel is 30 times bigger than the step height.

Dirichlet boundary condition is assumed for all variables, except pressure which is assumed by a zero-gradient condition, at the inlet. The kinetic energy of turbulence at the inlet is calculated from the experimental data of the inlet velocity fluctuations [30]. The turbulence dissipation rate at

Table 1. Parameter ξ for the fuzzy model.

Margin of β	Shear stress ($i \neq j$)	Normal stress ($i = j$)
$0 \leq \beta \leq 0.1$	$\xi = 0$	$\xi = 0$
$0.1 < \beta \leq 0.2$	$\xi = 0$	$\xi = 1$
$0.2 < \beta \leq 0.3$	$\xi = \beta$	$\xi = 1$
$0.3 < \beta$	$\xi = 1$	$\xi = 1$

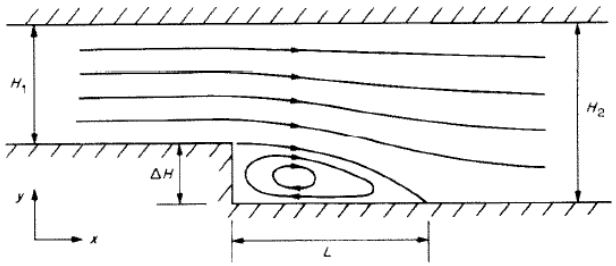

Figure 1. Schematic of the backward-facing step geometry.

the inlet is calculated by the following relation:

$$\varepsilon_{in} = \frac{k_{in}^{3/2}}{0.1 W_{in}} \tag{36}$$

where k_{in} is the inlet turbulence kinetic energy, and W_{in} is the inlet width (for a plane 2D case it is a unit length). The outflow boundary condition is considered at the outlet for turbulence variables. The outlet velocities are corrected via an overall mass balance, and a zero-pressure boundary condition is considered for the outlet cells. The no-slip boundary condition is assumed for solid walls.

Numerical simulations are performed with non-uniform grids of $(50*100)$, $(100*150)$, $(150*225)$, and $(175*250)$ to assess the grid-independency of the solution. The last two grids exhibit the same numerical solutions. Therefore, results based on $(150*225)$ grid is reported in the present paper. Figure 2 shows the non-uniform grids which is clustering at lower end with 1.2 of stretch factor. This helps to keep fine the near wall boundary grids in order to increase the accuracy of the solution in this area.

An important feature of the backward-facing step is the recirculation length, which is denoted by length L in Table 2 shows a comparison between the present simulations of the normalized recirculation length with the experimental data [30], and the numerical results of [31, 32]. As appears in the Table 2, the fuzzy model reproduces the same recirculation length as that of the experimental data. The present ASM (the WJ model) and binary model over-predict this length but are still closer to the experimental data than the ASM of [32]. The $k-\varepsilon$ model in the present code gives results like that of [30], which are considerably lower than the measured one.

Figure 3 shows the streamlines calculated by the ASM model of WJ. As can be seen, the ASM model of WJ has a better correspondence ($L/\Delta H = 7.2$) with experimental results than the result of the $k-\varepsilon$ model which, is shown in figure 4 for the recirculation length.

The calculated streamlines for the two blended models of binary and fuzzy models are shown in figure 5 and figure 6.

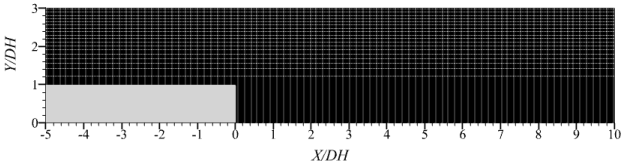

Figure 2. Backward-facing non-uniform grids.

Table 2. Normalized Recirculation Length ($L/\Delta H$) for the backward-facing step case.

Reference	Turbulence model	Normalized Recirculation Length ($L/\Delta H$)
Experiment [30]	———	7.0
Tangham & Speziale [31]	$k-\varepsilon$	6.25
Ahmadi & Chowdury [32]	ASM	6.5
Present Work	$k-\varepsilon$	6.2
Present Work	ASM (WJ)	7.2
Present Work	Binary	7.1
Present Work	Fuzzy	7.0

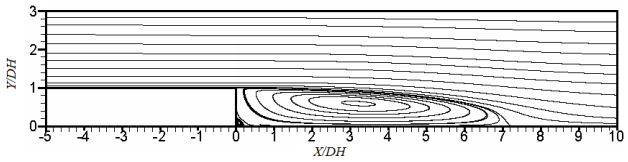

Figure 3. Streamlines calculated by the ASM model of WJ.

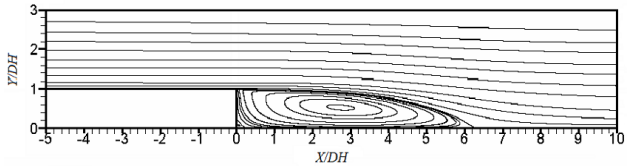

Figure 4. Streamlines calculated by the $k-\varepsilon$ model.

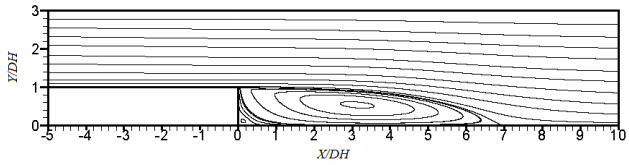

Figure 5. Streamlines calculated by the binary blended model.

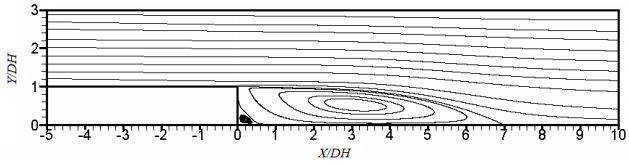

Figure 6. Streamlines calculated by the fuzzy blended model.

The binary model with the prediction of $L/\Delta H = 6.95$ and the fuzzy model with the prediction of $L/\Delta H = 7.0$ for the recirculation length have predicted very good results compared to the experimental results.

The profiles of normal and shear-turbulent stresses at different stations are shown in figures 7 to 12. Normal turbulent stress profiles of the aforementioned stations are shown in Figs. 7 to 9. The $k-\varepsilon$ model under-predicts the normal stresses at all three stations. The WJ model gives very good result for the first station but over-predicts normal stresses for other stations. Both blend models give overall good results for all stations, where the fuzzy model predictions are slightly better.

Profiles of turbulent shear stresses at stations $X/\Delta H =$ 7.667, 8.5, 10.333 are shown in figures 10 to 12. As seen in these figures, the WJ model over-predicts shear stresses, whereas the $k-\varepsilon$ model gives betters predictions. In fact, such behaviour has motivated the authors to search for a blend model. The $k-\varepsilon$ model slightly under-predicts the stresses at $X/\Delta H = 7.667$ and 10.333 but gives good prediction at $X/\Delta H = 8.5$. The binary model and the fuzzy

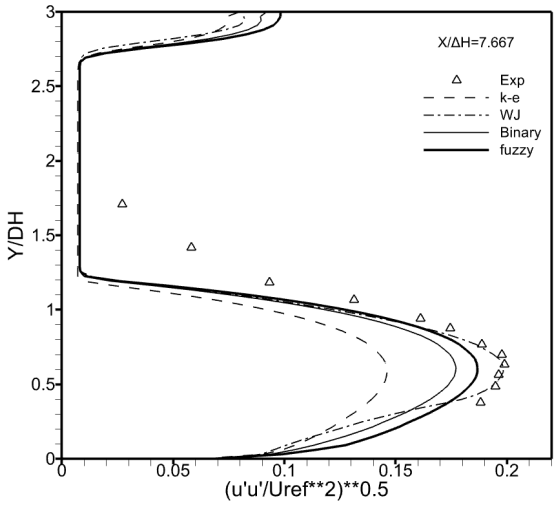

Figure 7. Non-dimensional turbulent normal stress at station $X/\Delta H = 7.667$.

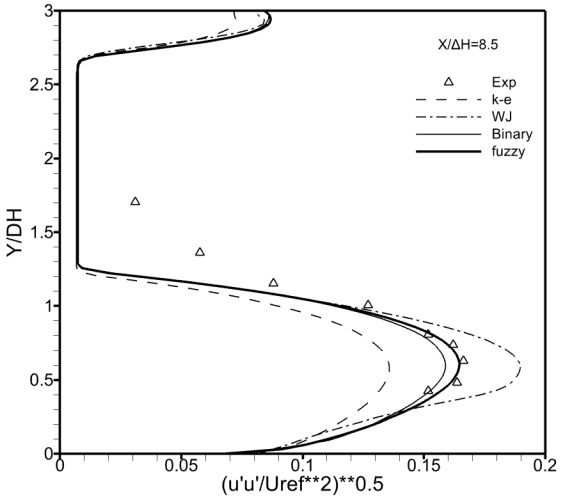

Figure 8. Non-dimensional turbulent normal stress at station $X/\Delta H = 8.5$.

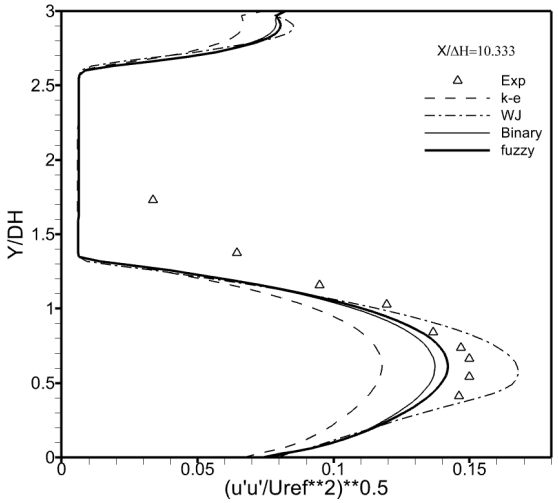

Figure 9. Non-dimensional turbulent normal stress at station $X/\Delta H = 10.333$.

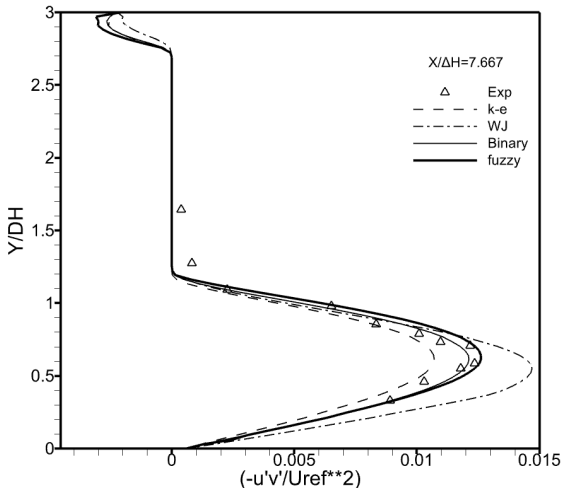

Figure 10. Non-dimensional turbulent shear stress at station $X/\Delta H = 7.667$.

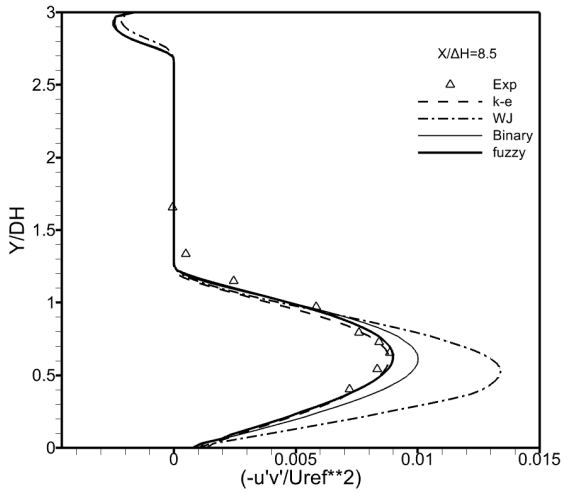

Figure 11. Non-dimensional turbulent shear stress at station $X/\Delta H = 8.5$.

model give good results at all stations, but the fuzzy model results are superior.

Note that there is a good correspondence between the abil-

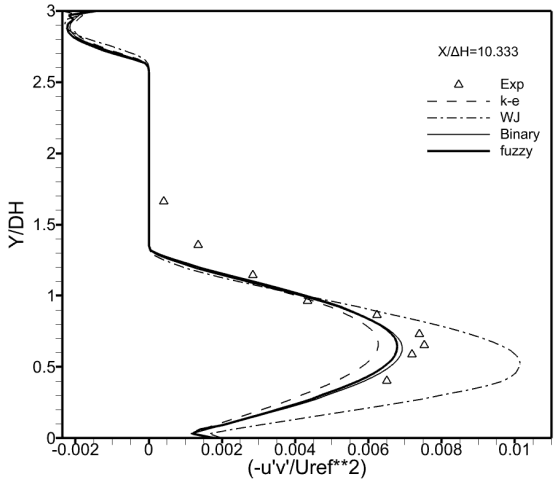

Figure 12. Non-dimensional turbulent shear stress at station $X/\Delta H = 10.333$.

ity of the turbulence model in predicting the reattachment point, see Table 2, and the shear stress profile near that region (station $X/\Delta H = 7.667$). As seen in figure 10, the WJ model over-predicts shear stress near the reattachment region, therefore resulting in an over-prediction of the reattachment point location. The $k-\varepsilon$ model under-predicts shear stress and consequently calculates a smaller length for the reattachment point. Both the blend models accurately predict the stress profiles and the reattachment length.

Table 3 shows the normalized CPU-time of each model. The values are normalized by the CPU-time of the $k-\varepsilon$ model. As appears in this table, the $k-\varepsilon$ model requires the minimum CPU-time to achieve convergence, which is an advantage of this model regarding computational economy. Both the blend models consume about 56% more CPU than the $k-\varepsilon$ model but still perform better than the WJ model which takes 76% more CPU time than the $k-\varepsilon$ model. Therefore, our goal to achieve more accurate results for both shear and normal turbulent stresses and consume less CPU time than that of more complex turbulence models seems to be fulfilled in this case.

Table 3. Normalized CPU time for different models for back-ward facing step simulations.

Turbulence Model	Normalized CPU
$k-\varepsilon$	1
WJ	1.76
Binary	1.56
Fuzzy	1.58

5. Conclusions

The limitations of the $k-\varepsilon$ model in accurately predicting turbulent normal stresses, despite its effectiveness in estimating turbulent shear stresses, led the authors to adopt a hybrid approach combining the $k-\varepsilon$ model with the WJ algebraic stress model. The study demonstrates that while the WJ model improves predictions for normal turbulent

stresses compared to the $k-\varepsilon$ model, its accuracy in predicting shear stresses is generally lower, and it demands significantly higher computational effort, requiring at least 75% more CPU time with weaker convergence behaviour. To address these challenges, blended models, including binary and fuzzy logic-based approaches, were explored. The results indicate that these blended models outperform both the $k-\varepsilon$ and WJ models in terms of accuracy for both normal and shear turbulent stresses. The fuzzy logic-based model, in particular, demonstrates enhanced adaptability by dynamically adjusting between the strengths of the $k-\varepsilon$ and WJ models, leading to more balanced and precise turbulence predictions. Additionally, these models exhibit improved convergence behaviour, and in the worst-case scenarios, their computational cost is at least 20% lower than that of the WJ model, making them a more efficient and reliable alternative for turbulence modelling. Future work could focus on extending these blended models to three-dimensional cases, incorporating more complex geometries, and further investigating their performance in practical applications such as industrial combustion or aero-thermal flows.

Availability of data and materials
The data that support the findings of this study are available from the corresponding author upon reasonable request.

Conflict of interests
The authors declare that they have no known competing financial interests or personal relationships that could have appeared to influence the work reported in this paper.

References

[1] J. Derek and B. Launder. Osborne reynolds and the publication of his papers on turbulent flow. *Annual Review of Fluid Mechanics*, 39: 1935, 2007.

[2] O. Darrigol. Joseph boussinesq's legacy in fluid mechanics. *Comptes Rendus Mécanique*, 345:427–445, 2017.

[3] W. Tollmien, H. Schlichting, H. Görtler, and F. W. Riegels. Über die ausgebildete turbulenz. in: Ludwig prandtl gesammelte abhandlungen: zur angewandten mechanik, hydro- und aerodynamik. *Springer*, page 736–751, 1961.

[4] K. Hanjalić and B. E. Launder. A reynolds stress model of turbulence and its application to thin shear flows. *Journal of Fluid Mechanics*, 52:609–638, 1972.

[5] J. Rotta. Statistische theorie nichthomogener turbulenz. *Zeitschrift Für Physik*, 129:547–572, 1951.

[6] B. E. Launder, G. J. Reece, and W. Rodi. Progress in the development of a reynolds-stress turbulence closure. *Journal of Fluid Mechanics*, 68:537–566, 1975.

[7] J. L. Lumley. Computational modeling of turbulent flows this work supported in part by the u.s. national science foundation, meteorology program under grant number atm77-22903, and in part by the u. s. office of naval research, fluid dynamics branch. it is a pleasure to acknowledge fruitful discussion with b. brumley, and the computational help of d. hatziavromidis. *Elsevier*, 1979.

[8] B. E. Launder. Phenomenological modelling: Presentand future. in: Whither turbulence turbulence at the crossroads. *Springer*, page 439–485, 1990.

[9] C. G. Speziale. Modeling the pressure gradient–velocity correlation of turbulence. *The Physics of Fluids*, pages 69–71, 1985.

[10] C. G. Speziale. Second-order closure models for rotating turbulent flows. *Quarterly of Applied Mathematics*, 45, 1987.

[11] D. C. Haworth and S. B. Pope. A generalized langevin model for turbulent flows. *The Physics of Fluids*, 29:387–405, 1986.

[12] W. Rodi. A new algebraic relation for calculating the reynolds stresses. *Gesellschaft Angewandte Mathematik und Mechanik Workshop Paris France*, 56:219, 1976.

[13] C. G. Speziale, S. Sarkar, and T. B. Gatski. Modelling the pressure–strain correlation of turbulence: an invariant dynamical systems approach. *Journal of Fluid Mechanics*, 227:245–272, 1991.

[14] S. T. Wallin and A. V. Johansson. An explicit algebraic reynolds stress model for incompressible and compressible turbulent flows. *Journal of Fluid Mechanics*, 403:89–132, 2000.

[15] L. Davidson. Second-order corrections of the $k-\varepsilon$ model to account for non-isotropic effects due to buoyancy. *International Journal of Heat and Mass Transfer*, 33:2599–2608, 1990.

[16] F. R. Menter. Two-equation eddy-viscosity turbulence models for engineering applications. *Advancement of the Science and Technology of Astronautics and Aeronautics Journal*, 32:1598–1605, 1994.

[17] D. C. Wilcox. Reassessment of the scale-determining equation for advanced turbulence models. *Advancement of the Science and Technology of Astronautics and Aeronautics Journal*, 26:1299–1310, 1988.

[18] Khaleghi and E. Fallah. Iterative and non-iterative solutions of engine flows using asm and $k-e$ turbulence models. *Annual conference of the CFD Society of Canada*, pages 493–500, 2003.

[19] B. Basara and S. Jakirlic. A new hybrid turbulence modelling strategy for industrial cfd. *International Journal for Numerical Methods in Fluids*, 42:89–116, 2003.

[20] E. Lynch and M. Smith. Hybrid rans-les turbulence models on unstructured grids. *38th Fluid Dynamics Conference and Exhibit*, AIAA-2008-3854, 2008.

[21] A. Islam and B. Thornber. A high-order hybrid turbulence model with implicit large-eddy simulation. *Computers & Fluids*, 167:292–312, 2018.

[22] G. Alfonsi. Reynolds-averaged navier-stokes equations for turbulence modeling. *Applied Mechanics Reviews*, 62, 2009.

[23] W. P. Jones and B. E. Launder. The prediction of laminarization with a two-equation model of turbulence. *International Journal of Heat and Mass Transfer*, 15:301–314, 1972.

[24] T. B. Gatski and C. G. Speziale. On explicit algebraic stress models for complex turbulent flows. *Journal of Fluid Mechanics*, 254:59–78, 1993.

[25] P. Hájek. What is mathematical fuzzy logic. *Fuzzy Sets and Systems*, 157:597–603, 2006.

[26] Y. S. Perera, J. Li, and C. Abeykoon. Adaptive neuro-fuzzy controller for real-time melt pressure control in polymer extrusion processes. *European Control Conference (ECC)*, pages 2023–2028, 2024.

[27] A.-T. Nguyen, T. Taniguchi, L. Eciolaza, V. Campos, R. Palhares, and M. Sugeno. Fuzzy control systems: Past, present and future. *IEEE Computational Intelligence Magazine*, 14:56–68, 2019.

[28] F. P. Nishanth, S. K. Dash, and S. R. Mahapatro. Critical study of type-2 fuzzy logic control from theory to applications: A state-of-the-art comprehensive survey. *e-Prime - Advances in Electrical Engineering, Electronics and Energy*, 10:100771, 2024.

[29] S. Patankar. Numerical heat transfer and fluid flow. *McGraw Hill*, 1980.

[30] J. Kim, S. J. Kline, and J. P. Johnston. Investigation of a reattaching turbulent shear layer: Flow over a backward-facing step. *Journal of Fluids Engineering-transactions of The Asme*, 102:302–308, 1980.

[31] N. Hur, S. Thangam, and C. Speziale. Numerical study of turbulent secondary flows in curved ducts. *Journal of Fluids Engineering*, 112, 1990.

[32] G. Ahmadi and S. J. Chowdhury. A rate-dependent algebraic stress model for turbulence. *Applied Mathematical Modelling*, 15:516–524, 1991.